JACS
JOURNAL OF THE AMERICAN CHEMICAL SOCIETY
Article
pubs.acs.org/JACS

Polyoxometalate-Based Nickel Clusters as Visible Light-Driven Water Oxidation Catalysts

Xin-Bao Han, Yang-Guang Li,* Zhi-Ming Zhang, Hua-Qiao Tan, Ying Lu, and En-Bo Wang*

Key Laboratory of Polyoxometalate Science of the Ministry of Education, Faculty of Chemistry, Northeast Normal University, Changchun, Jilin 130024, P.R. China

Supporting Information

ABSTRACT: Three new polyoxometalate(POM)-based polynuclear nickel clusters, $Na_{24}[Ni_{12}(OH)_9(CO_3)_3(PO_4)(SiW_9O_{34})_3]\cdot 56H_2O$ (**1**), $Na_{25}[Ni_{13}(H_2O)_3(OH)_9(PO_4)_4(SiW_9O_{34})_3]\cdot 50H_2O$ (**2**), and $Na_{50}[Ni_{25}(H_2O)_2OH)_{18}(CO_3)_2(PO_4)_6(SiW_9O_{34})_6]\cdot 85H_2O$ (**3**) were synthesized and structurally characterized. Compounds **1**−**3** contain $\{Ni_{12}\}$, $\{Ni_{13}\}$ and $\{Ni_{25}\}$ core, respectively, connected by the inorganic {OH}, $\{PO_4\}$ and/or $\{CO_3\}$ linkers and encapsulated by the lacunary *A*-*α*-$\{SiW_9O_{34}\}$ POM units. Compound **3** represents the currently largest POM-based Ni clusters. All three compounds contain $\{Ni_3O_3\}$ quasi-cubane or $\{Ni_4O_4\}$ cubane units, which are similar to the natural oxygen-evolving center $\{Mn_4O_5Ca\}$ in photosystem II (PSII). Visible light-driven water oxidation experiments with compounds **1**−**3** as the homogeneous catalysts indicate that all three compounds show good photocatalytic activities. The O_2 evolution amount corresponds to a high TON of 128.2 for **1**, 147.6 for **2**, and 204.5 for **3**, respectively. Multiple experiments including dynamic light-scattering, UV−vis absorption, catalysts aged experiments, tetra-*n*-heptylammonium nitrate ($THpANO_3$) toluene extraction, and capillary electrophoretic measurements results confirm that compounds **1**−**3** are dominant active catalysts but not Ni^{2+} ions(aq) or nickel oxide under the photocatalytic conditions. The above research results indicate a new and all-inorganic polynuclear Ni-based structural model as the visible light-driven water oxidation catalysts.

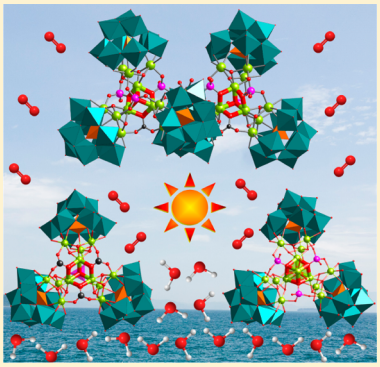

INTRODUCTION

The solar-driven production of H_2 and O_2 from water based on earth-abundant materials represents a promising and desirable approach to sustainably provide clean and renewable fuel. In this research field, the exploration of new water oxidation catalysts (WOCs) is a challenging work, and substantial work has been started in past few years.[1−7] In particular, molecular catalysts with cheap and abundant elements as well as well-defined structures are currently a major focus since they may aid in tuning of oxygen evolution performances at the molecular level and simulating the natural oxygen evolving center $\{Mn_4O_5Ca\}$ with low-cost to meet global energy demands.[8−11] Over the past few years, many significant molecular WOCs based on manganese,[12,13] iron,[14,15] cobalt,[16,17] nickel,[18,19] and copper[20,21] elements have been explored in oxidizing water to produce oxygen under photo- or electrochemical conditions. Among these first-row transition metal (TM) elements, nickel is the ninth most abundant element in the Earth's crust and Ni-based materials have been theoretically estimated to be one of significant WOCs due to their matchable water oxidation potential.[22,23] However, little success has been achieved for the synthesis of efficient Ni-based WOCs in contrast to other TM-based WOCs.

Polyoxometalates (POMs) have recently been proven as one kind of ideal inorganic ligand to design and synthesize new WOCs.[24−43] POMs, as one class of unique metal-oxo clusters with well-defined structures and nano size, are composed of W, Mo, V, Nb, and Ta centers with their highest oxidation states.[44−48] Such clusters are generally oxidatively resistant, and their oxygen-rich surfaces can be viewed as multidentate O-donor ligands to construct various TM clusters.[49,50] Noticeably, the introduction of TM into POMs can help tune the band gap structures and even broaden the spectrum absorption of such molecular clusters from UV to visible light region.[31,41,43,51] Moreover, POMs possess multiple redox active metal sites and can maintain their structural integrity under the photocatalytic conditions.[26,31,38−41] As a consequence, a number of stable and robust POM-based WOCs have recently been explored, including the POM-based Ru, Co and Mn clusters.[24−27,29,52,53]

However, the POM-based nickel WOCs have been far unexplored.[8,35] In many POM-based WOCs, an important $\{M_4O_4\}$ cubane and/or $\{M_3O_3\}$ quasi-cubane core has been noticed, which not only may structurally simulate the natural oxygen-evolving center $\{Mn_4O_5Ca\}$,[54] but also might play a key role in light-driven water oxidation process. In our previous work, we have explored a series of POM-based cobalt−phosphate WOCs with $\{Co_4O_4\}$ cubane core.[39] In the light of above consideration, we attempt to construct new POM-based Ni clusters with $\{Ni_4O_4\}$ cubane and/or $\{Ni_3O_3\}$ quasi-cubane cores so as to mimic the natural oxygen-evolving center $\{Mn_4O_5Ca\}$ and explore new type of WOCs.

Received: February 6, 2015
Published: April 13, 2015

DOI: 10.1021/jacs.5b01329
J. Am. Chem. Soc. 2015, 137, 5486−5493

Herein, we report three new POM-based polynuclear nickel clusters: $Na_{24}[Ni_{12}(OH)_9(CO_3)_3(PO_4)(SiW_9O_{34})_3]\cdot 56H_2O$ (**1**), $Na_{25}[Ni_{13}(H_2O)_3(OH)_9(PO_4)_4(SiW_9O_{34})_3]\cdot 50H_2O$ (**2**), and $Na_{50}[Ni_{25}(H_2O)_2(OH)_{18}(CO_3)_2(PO_4)_6(SiW_9O_{34})_6]\cdot 85H_2O$ (**3**). Compounds **1**−**3** exhibit a series of polynuclear Ni clusters connected by the inorganic {OH}, {PO_4} and/or {CO_3} linkers and encapsulated by the lacunary *A*-*α*-{SiW_9O_{34}} POM units. Compound **3** represents the currently largest POM-based Ni cluster. It is noteworthy that all three compounds contain {Ni_3O_3} quasi-cubane or {Ni_4O_4} cubane core, which are similar to the cubical {Mn_4O_5Ca} cluster of the oxygen evolving center in PSII. The visible light-driven water oxidation experiments with compounds **1**−**3** as the homogeneous catalysts have been investigated. All three compounds show good photocatalytic activities. The O_2 evolution amount corresponds to a high TON (defined as $n(O_2)/n$(catalyst)) of 128.2 for **1**, 147.6 for **2**, and 204.5 for **3**, respectively. Furthermore, the stability of compounds **1**−**3** in the catalytic system was also examined in detail.

EXPERIMENTAL SECTION

Materials and Methods. $Na_{10}[A\text{-}\alpha\text{-}SiW_9O_{34}]\cdot 18H_2O$ was synthesized according to the literature method.[55] $[Ru(bpy)_3]Cl_2\cdot 6H_2O$ and $Na_2S_2O_8$ were purchased from Aldrich. Other chemicals used for the syntheses were of the reagent grade available from commercial sources. Elemental analyses of Ni, W, and Na were performed on a PLASMA-SPEC (I) inductively coupled plasma (ICP) atomic emission spectrometer. IR spectra were recorded in the range of 400−4000 cm^{-1} on an Alpha Centaurt FT-IR Spectrophotometer. Thermogravimetric analyses were performed on a Perkin−Elmer TGA7 instrument in N_2 atmosphere with a heating rate of 5 °C·min^{-1}. UV/vis absorption spectra were measured by using a U-3010 spectrophotometer (Hitachi, Japan). Dynamic light scattering (DLS) measurements were performed on a Zatasizer Nano 3600 instrument (Malven Instrument Co.). Cyclic voltammetry (CV) experiments were performed with a CHI660C Electrochemical Analyzer (CH Instruments, China). The capillary electrophoretic experiments were performed in a capillary electrophoretic apparatus (CL1020 Beijing Cailu Science Apparatus, China) under 22 °C cooling air with the UV detector. Single crystal data were collected on a Bruker Apex CCD diffractometer for **1**−**3**. Suitable crystals were mounted in a thin-glass tube and transferred to the goniostat. The structures of **1**−**3** were solved by the direct method and refined by the full-matrix least-squares fit on F^2 using the SHELXTL-97 crystallographic software package.[56]

Synthesis of ***1****.* $NiCl_2\cdot 6H_2O$ (0.67 g, 2.78 mmol) was dissolved in 40 mL of distilled water. $Na_{10}[A\text{-}\alpha\text{-}SiW_9O_{34}]\cdot 18H_2O$ (1.0 g, 0.34 mmol) was added and the mixture was stirred until a light cloudy, green solution was obtained. $Na_3PO_4\cdot 12H_2O$ (0.80 g, 2.1 mmol) and Na_2CO_3 (0.10 g, 0.94 mmol) was added successively, and then 210−315 μL of 4.0 M HCl (aq) was added dropwise so as to adjust the pH in the range of 8.0−9.0. The resulting green mixture was stirred for 3 h at room temperature and then the light green precipitate was removed by filtration. The filtrate was kept in a 50 mL beaker to allow slow evaporation at room temperature. After 1 or 2 weeks, green block crystals suitable for X-ray crystallography were obtained, washed with cold distilled water, and dried in the air to give 186 mg of **1** (16.5% yield, based on tungstate). Anal. Calcd (%): Na, 5.89; Ni, 7.51; W, 52.9. Found: Na, 5.93; Ni, 7.59; W, 52.6. IR (KBr disks): 1092 (s), 981 (s), 929 (s), 852 (m), 798 (w), 755 (w), 646 (w), and 504 cm^{-1} (w).

Synthesis of ***2****.* $NiCl_2\cdot 6H_2O$ (0.4 g, 1.68 mmol) was dissolved in 40 mL of distilled water. $Na_{10}[A\text{-}\alpha\text{-}SiW_9O_{34}]\cdot 18H_2O$ (1.0 g, 0.34 mmol) was added and this mixture was stirred until a clear, green solution was obtained. Then, $Na_3PO_4\cdot 12H_2O$ (0.80 g, 2.1 mmol) was added and the above mixture was adjusted to pH of 8.0−9.0 with 200−305 μL of 4.0 M HCl (aq). The resulting turbid solution was stirred for 2 h at 80−90 °C and the green precipitate was removed by filtration. The filtrate was kept in a 50 mL beaker to allow slow evaporation at room temperature. After 2 weeks, green block crystals suitable for X-ray crystallography were obtained, washed with cold distilled water, and dried in the air to give 200 mg of **2** (17.6% yield, based on tungstate). Anal. Calcd (%) for **2**: Na, 6.05; Ni, 8.03; W, 52.2. Found: Na, 5.98; Ni, 7.94; W, 52.0. IR (KBr pellet) for **2**: $\tilde{U}$ = 1098 (s), 983 (s), 929 (s), 851 (m), 802 (m), 756 (w), 655 (w), 578 (w), and 491 cm^{-1} (w).

Synthesis of ***3****.* $NiCl_2\cdot 6H_2O$ (0.3 g, 1.26 mmol) was dissolved in 40 mL of distilled water. $Na_{10}[A\text{-}\alpha\text{-}SiW_9O_{34}]\cdot 18H_2O$ (1.0 g, 0.34 mmol) was added and this mixture was stirred until a clear, green solution was formed. Then, $Na_3PO_4\cdot 12H_2O$ (0.80 g, 2.1 mmol) and Na_2CO_3 (0.05 g, 0.47 mmol) were added successively, followed by the adjustment of pH of 8.0−9.0 with 255−325 μL of 4.0 M HCl (aq). The resulting green mixture was stirred for 2 h at 60−70 °C and the green precipitate was removed by filtration. The filtrate was kept in a 50 mL beaker to allow slow evaporation at room temperature. After 3 weeks, green block crystals suitable for X-ray crystallography were isolated, washed with cold distilled water, and air-dried to give 100 mg of **3** (9.0% yield, based on tungstate). Anal. Calcd (%) for **3**: Na, 6.20; Ni, 7.91; W, 53.5. Found: Na, 6.12; Ni, 7.78; W, 53.3. IR (KBr pellet) for **3**: $\tilde{U}$ = 1103 (s), 1517 (m), 982 (s), 930 (s), 850 (m), 797 (m), 653 (w), 586 (w) and 510 cm^{-1} (w).

Photocatalytic Water Oxidation Measurements. Visible light-driven water oxidation was performed in an external illumination type reaction vessel (total volume 100 mL) with a magnetic stirrer for vigorous stirring and analyzed by using an automatic O_2 monitoring system at room temperature. The vessel was filled with 20 mL of reaction solution with different concentrations of **1**−**3** (0−10 μM), sacrificial electron acceptor $Na_2S_2O_8$ (5 mM), and photosensitizer $[Ru(bpy)_3]Cl_2$ (1 mM) in borate buffer solution (80 mM, pH 9.0). Before irradiation, the reaction solution was first degassed by ultrasonication and added to the photosensitizer $[Ru(bpy)_3]Cl_2$, then evacuated in the dark to ensure complete air removal. The photoirradiation was performed using a 300 W Xe lamp equipped with a long-pass filter (420 nm cutoff). The produced O_2 was analyzed by gas chromatography with a GC7890T instrument with a thermal conductivity detector (TCD) and a 5 Å molecular sieve column (2 m × 3 mm) using Ar as carrier gas.

RESULTS AND DISCUSSION

Synthesis and Structures of 1−3. During the synthesis of compounds **1**−**3**, several important synthetic factors should be emphasized. First, the pH of reaction solution should be in the range of 8.0−9.0, which is the suitable condition for the assembly of compounds **1**−**3**. Out of such pH range, no crystalline products were obtained in such reaction system. Second, the reaction temperature and the use of different amount of Na_2CO_3 may play important roles in assembling the final different crystal structures of **1**−**3**. Compound **1** was synthesized at room temperature, but if the Na_2CO_3 was not introduced into the reaction system, compound **1** cannot be obtained. The reaction system of compound **2** should be heated at 80−90 °C for 2 h so as to isolate the crystalline products. In this case, no Na_2CO_3 was used. Thus, the {Ni_{13}} core in compound **2** was encapsulated by pure {PO_4} ligands and {*A*-*α*-SiW_9O_{34}} units. The relatively high reaction temperature is an essential condition since no crystalline compound was prepared at room temperature in this case. Compound **3** was prepared at 60−70 °C for 2 h with the addition of Na_2CO_3. Without heating, no crystalline product of compound **3** is isolated from the reaction system. Furthermore, if no Na_2CO_3 was added, very low yield (less than 2%) of compound **3** is synthesized in such reaction system. On the basis of above synthetic conditions and the crystal structures of compounds **1**−**3**, it is envisioned that the inorganic PO_4^{3-} ligands might be activated by heating to coordinate with central Ni cores. However, the inorganic CO_3^{2-} ligands seem to be more active

DOI: 10.1021/jacs.5b01329
J. Am. Chem. Soc. 2015, 137, 5486−5493

than PO_4^{3-} to link with Ni cores at room temperature. Finally, the molar ratio of the precursors Ni^{2+} and {*A*-*α*-PW_9O_{34}} seems to be a noncrucial factor for the final assembly of compounds **1**−**3**, since various molar ratios such as 8.2:1, 4.9:1 and 3.7:1 can all be feasible for the preparation of POM-based Ni clusters. However, the use of excessive nickel salts may lead to large amount of insoluble green precipitate with PO_4^{3-}. Especially in the reaction system of compound **1**, such reaction may decrease the content of PO_4^{3-} in reaction system and lead to more CO_3^{2-} ligands linked with the central Ni cluster. On the basis of above experiments, it is found that compounds **1**−**3** were synthesized in similar reaction conditions. However, if the reaction conditions were carefully controlled, especially the reaction temperature and the use of different amount of Na_2CO_3, three different compounds with high yield and purity can be obtained. The main synthetic conditions and differences of compounds **1**−**3** are shown in Figure 1.

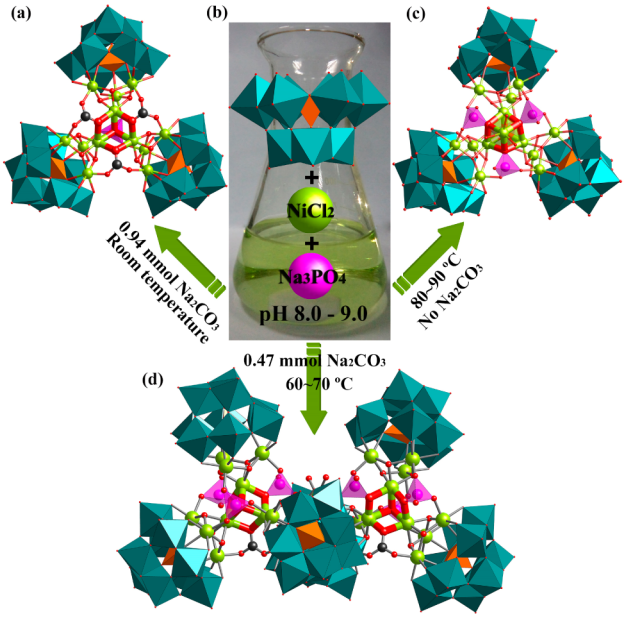

Figure 1. Synthetic route to obtain compounds **1**−**3**. Ball-and-stick and polyhedral representation of the polyoxoanion structures of compounds (a) **1**, (c) **2** and (d) **3**; (b) Schematic view of the synthetic system. WO_6, teal octahedra; PO_4, pink tetrahedra; SiO_4, orange tetrahedra; C, black sphere; O, red sphere; Ni, lime sphere.

Single crystal X-ray diffraction analysis showed that compound **1** crystallizes in the triclinic space group $P\bar{1}$. The polyoxoanion **1a** contains three lacunary *A*-*α*-{SiW_9O_{34}} POM units and one central {$Ni_{12}(OH)_9(CO_3)_3(PO_4)$} ({$Ni_{12}$}) moiety (see Figure 2a and 2b). The central {Ni_{12}} cluster can be described as four tetrahedral {$Ni_4(OH)_3$} fragments connected by three μ_3-{CO_3} linkers and one μ_4-{PO_4} linker. Furthermore, the {Ni_{12}} core was encapsulated by three *A*-*α*-{SiW_9O_{34}} units (see Figure 2c). From another point of view, the polyoxoanion **1a** possesses a central {$Ni_3(CO_3)_3(PO_4)$} core, which is encapsulated by three {(*A*-*α*-SiW_9O_{34})$(NiOH)_3$} units (see Figure 2d and 2e). Such a {$Ni_3(CO_3)_3(PO_4)$} core exhibits a {Ni_3O_3} quasi-cubane unit (see Figure 2f), which is structurally similar to the natural oxygen-evolving {Mn_4O_5Ca} center. In the {Ni_3O_3} quasi-cubane, the Ni−O distances are in the range of 2.020(17)−2.18(2) Å and the Ni···Ni distances range from 3.2009(62) to 3.2206(53) Å. Bond valence sum

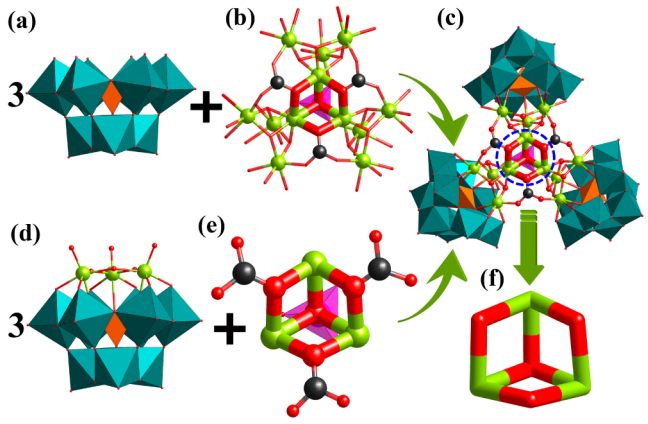

Figure 2. Polyhedral and ball-and-stick representation of the polyoxoanion **1a** and various building blocks (a), (b), (d), and (e) of compound **1**; ball-and-stick representation of {Ni_3O_3} quasi-cubane core (f) in **1a**. WO_6, teal octahedra; SiO_4, orange tetrahedra; PO_4, pink tetrahedra; O, red sphere; C, black sphere; Ni, lime sphere.

(BVS) calculations indicated that all the nickel ions are in the +2 oxidation state. In our previous work, we have ever reported another {Ni_{12}} cluster, which is encapsulated by three lacunary *B*-*α*-{SiW_9O_{34}} POM units, one {$W_7O_{26}(OH)$} moiety and one {WO_4} fragment, but no μ_3-{CO_3} and/or μ_4-{PO_4} linkers were introduced into such POM-based {Ni_{12}} cluster.[57] It is also worth mentioning that Kortz et al. have recently reported a POM-based {Ni_{14}} cluster. Such a {Ni_{14}} compound can be viewed as four {(*B*-*α*-$P_2W_{15}O_{56}$)$(NiOH)_3$} units connected by a dinuclear {$Ni_2(H_2O)_2$} moiety and four {PO_4} linkers.[58]

Compound **2** crystallizes in the monoclinic space group *P*2(1)/*n*. The polyoxoanion **2a** consists of one central {$Ni_{13}(H_2O)_3(OH)_9(PO_4)_3$} ({$Ni_{13}$}) fragment and three lacunary *A*-*α*-{SiW_9O_{34}} POM units (see Figure 3a and 3b). The central {Ni_{13}} core is structurally similar to {Ni_{12}} core in the polyoxoanion **1a** except that an extra {$Ni(H_2O)_3$} fragment entered into the central core (see Figure S2a and S2b, Supporting Information (SI)) and such {Ni_{13}} core is linked by three μ_3-{PO_4} linkers and one μ_4-{PO_4} linker. The whole {Ni_{13}} cluster is well encapsulated by three *A*-*α*-{SiW_9O_{34}}

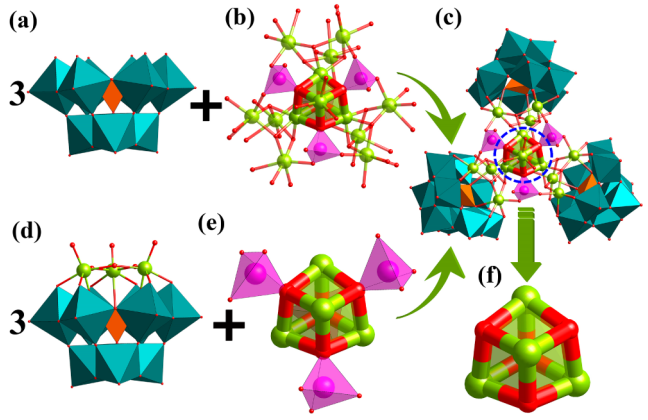

Figure 3. Polyhedral and ball-and-stick representation of the polyoxoanion **2a** and its building blocks (a), (b), (d), and (e) of compound **2**; Ball-and-stick representation of {Ni_4O_4} cubane core (f) in **2a**. WO_6, teal octahedra; SiO_4, orange tetrahedra; PO_4, pink tetrahedra; O, red sphere; Ni, lime sphere.

DOI: 10.1021/jacs.5b01329
J. Am. Chem. Soc. 2015, 137, 5486−5493

moieties (see Figure 3c). From another point of view, the polyoxoanion **2a** can also be viewed as a central $\{Ni_4(H_2O)_3(PO_4)_4\}$ core wrapped by three $\{(A\text{-}\alpha\text{-}SiW_9O_{34})(NiOH)_3\}$ units (see Figure 3d and 3e). Such a $\{Ni_4(H_2O)_3(PO_4)_4\}$ core comprises a central $\{Ni_4O_4\}$ cubane unit, which is reminiscent of that of the $\{Mn_4O_5Ca\}$ active site of the oxygen-evolving center in PSII (see Figure 3f). In the $\{Ni_4O_4\}$ cubane, the Ni−O distances are in the range of 2.043(15)−2.148(14) Å and the Ni···Ni distances range from 3.1677(45) to 3.2094(42) Å. Bond valence sum (BVS) calculations indicated that all the nickel ions are in the +2 oxidation state. To our knowledge, such a polynuclear $\{Ni_{13}\}$ core is observed for the first time in the POM-based Ni clusters.[49,50]

Compound **3** crystallizes in the triclinic space group $P\bar{1}$. The polyoxoanion **3a** is constructed by a $\{Ni_{25}(H_2O)_2(OH)_{18}(CO_3)_2(PO_4)_6\}$ ($\{Ni_{25}\}$) core and six lacunary $A\text{-}\alpha\text{-}\{SiW_9O_{34}\}$ POM units (see Figure 4a and 4c). The central $\{Ni_{25}\}$ cluster

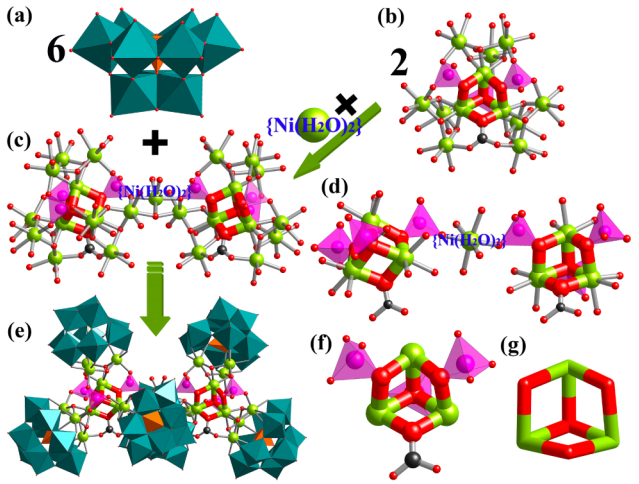

Figure 4. Polyhedral and ball-and-stick representation of the building blocks (a), (c), (d), (f) and polyoxoanion **3a** (e) of compound **3**; ball-and-stick representation of $\{Ni_{12}(OH)_9(CO_3)(PO_4)_3\}$ moiety of the $\{Ni_{25}\}$ core fragment (b); ball-and-stick representation of the $\{Ni_3O_3\}$ quasi-cubane unit (g) in compound **3**. WO_6, teal octahedra; NiO_6, lime octahedra; PO_4, pink tetrahedra; SiO_4, orange tetrahedra; O, red sphere; C, black sphere; Ni, lime sphere.

can be viewed as two $\{Ni_{12}(OH)_9(CO_3)(PO_4)_3\}$ moieties connected together by a $\{Ni(H_2O)_2\}$ linker (see Figure 4b). Each $\{Ni_{12}(OH)_9(CO_3)(PO_4)_3\}$ unit in **3a** is quite similar to the central $\{Ni_{12}\}$ core of **1a** except that $\{Ni_{12}\}$-**3a** core is linked by one μ_3-$\{CO_3\}$ linker, two μ_3-$\{PO_4\}$ linkers and one μ_4-$\{PO_4\}$ linker (see Figure 4b, Figure S2a, S2c and S2d in SI). The whole $\{Ni_{25}\}$ cluster is well encapsulated by six $A\text{-}\alpha\text{-}\{SiW_9O_{34}\}$ moieties (see Figure 4e). From another point of view, the polyoxoanion **3a** contains two $\{Ni_3(CO_3)(PO_4)_3\}$ cores wrapped by six $\{(A\text{-}\alpha\text{-}SiW_9O_{34})(NiOH)_3\}$ units (see Figure 4d). Each $\{Ni_3(CO_3)(PO_4)_3\}$ core comprises a $\{Ni_3O_3\}$ quasi-cubane unit, which is structurally similar to the natural oxygen-evolving $\{Mn_4O_5Ca\}$ center (see Figure 4g). The Ni−O distances are in the range of 1.997(12)−2.134(13) Å and the Ni···Ni distances range from 3.1681(1) to 3.2135(1) Å. BVS calculations indicated that all the nickel ions are in the +2 oxidation state. To our knowledge, the polyoxoanions **3a** represents the currently largest POM-based Ni clusters in POM chemistry.

Visible Light-Driven Water Oxidation by 1−3. The visible light-driven water oxidation activities of compounds **1**−**3** were investigated in the $[Ru(bpy)_3]^{2+}$/visible-light illumination/$Na_2S_2O_8$ water oxidation system. In this water-oxidation system, $[Ru(bpy)_3]^{2+}$ was used as photosensitizer, $S_2O_8^{2-}$ as sacrificial electron acceptor and compounds **1**−**3** as the catalysts for oxygen evolution from water under visible-light illumination. The proposed mechanism for the water oxidation systems catalyzed by **1**−**3** under the visible light irradiation were depicted in Scheme S1 in SI.[59,60] The photocatalytic water oxidation was investigated with 20 mL of reaction solution at different concentrations of **1**−**3** (0−10 μM), and their photocatalytic performances are shown in Figure 5 and Table S5 in SI. The O_2 rapidly evolved after 5 min of visible light illumination and the O_2 evolution amount was analyzed by online GC. The O_2 evolution rate of all these reactions decreased over time and a maximum value of O_2 yield (15.1% for **1**, 15.5% for **2**, and 17.6% for **3**) and O_2 evolution amount (7.54 μmol for **1**, 7.73 μmol for **2**, and 8.78 μmol for **3**) were achieved for 0.2 μmol of **1**−**3** (10 μM) after 60 min illumination (see Table S5, SI). The O_2 evolution amount corresponds to a high TON of 128.2 for **1**, 147.6 for **2**, and 204.5 for **3**, respectively (see Table S5 and Figure S4, SI). Accordingly, it was found that the photocatalytic efficiencies of **1**−**3** follow the order of **1** < **2** < **3** (see Figure 5 and Table S5 in SI). Also, the initial rate of photocatalytic water oxidation was in agreement with the above sequence of the catalytic activities of catalysts **1**−**3**. The O_2 yield increased as the catalyst concentrations increased and the TON decreased from 128.2 to 37.7 for **1**, from 147.6 to 38.6 for **2**, and from 204.5 to 43.9 for **3**, respectively, with their concentration increasing from 1 to 10 μM (see Table S5 and Figure S4, SI). Moreover, when the concentration of **1**−**3** increased from 5 to 10 μM, the O_2 evolution amount did not obviously increase.

It is noteworthy that quite little insoluble substance was observed after the catalytic reaction with 10 μM of **1**−**3**, which was not observed at low catalyst concentrations ($\leq$5 μM). The DLS results showed no particles can be detected by using 5 μM **1**−**3** and 700−900 nm particles were detected with 10 μM **1**−**3** after photocatalytic water oxidation (see Figure S14 and S15, SI). This phenomenon indicates the formation of POM-$Ru(bpy)_3$ composite precipitates, which leads to a low concentration of POM catalysts in actual catalytic system in contrast to the theoretical value. Thus, the TON of compounds **1**−**3** decrease as the amount of catalysts increases.[31,35,38−40] The EDX analyses of these ion pairing salt precipitates indicated the presence of Ru, W, Ni, and P (Figure S11, SI). An initial turnover frequency (TOF) in the first 300 s reached 0.20, 0.25, and 0.34 s^{-1} for compounds **1**, **2**, and **3**, respectively. Herein, the initial TOF for oxygen evolution is defined as $TOF_{initial}$ = mol of O_2/(mol of catalyst × 300 s), based on the amount of evolution O_2 after 300 s of visible-light irradiation. These TON and TOF values are comparable to the reported Ru- and Co-containing POM-based WOCs,[26,31,33,35] and compound **3** represents currently the most active nickel-containing POM water oxidation photocatalyst (see Table S6, SI).

We also compared the photocatalytic activities of the sandwich-type POM-based $\{Ni_4\}$ compounds $[Ni_4(H_2O)_2(PW_9O_{34})_2]^{10-}$ and $[Ni_4(H_2O)_2(SiW_9O_{34})_2]^{12-}$ under the same reaction conditions applied for **1**−**3**. However, no photocatalytic activity was observed under our conditions (see Table 1). Patzke and co-workers also found that the

DOI: 10.1021/jacs.5b01329
J. Am. Chem. Soc. 2015, 137, 5486−5493

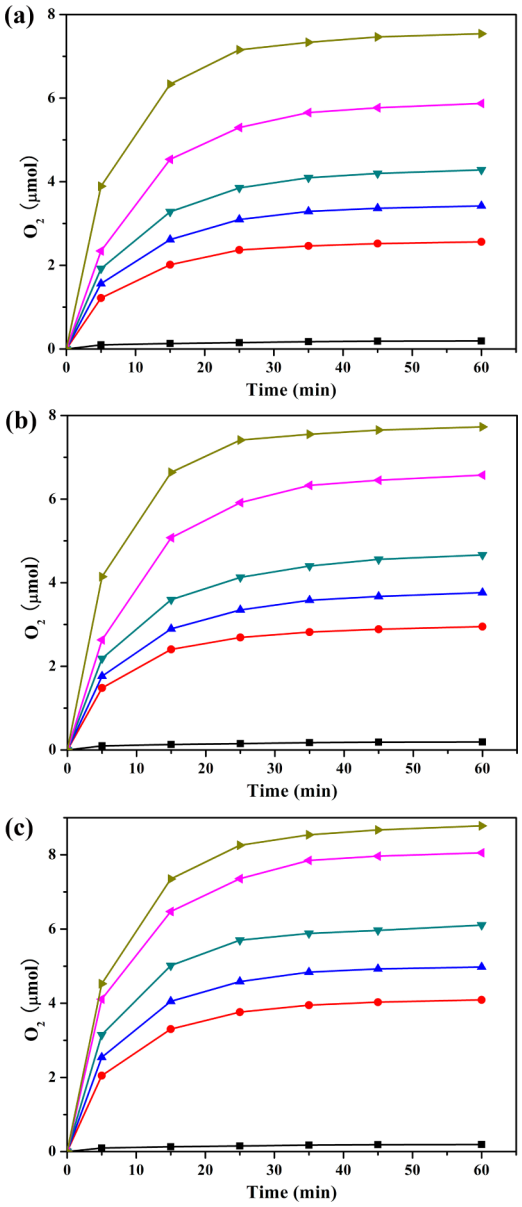

Figure 5. Kinetics of O_2 evolution in the photocatalytic system at different concentrations of (a) **1**; (b) **2**; and (c) **3**. The symbols used to denote catalyst concentrations are 0 μM (black ■), 1 μM (red ●), 2 μM (royal blue ▲), 3 μM (teal blue ▼), 5 μM (magenta left-pointing triangle), and 10 μM (olive right-pointing triangle). Conditions: 300 W Xe lamp equipped with a long-pass filter (420 nm cutoff); 1.0 mM $[Ru(bpy)_3]Cl_2$, 5.0 mM $Na_2S_2O_8$, sodium borate buffer pH 9.0 (80 mM); total reaction volume 20 mL; vigorous stirring (1.5×10^3 rpm).

$[Ni_4(H_2O)_2(SiW_9O_{34})_2]^{12-}$ did not display any photocatalytic O_2 evolution activity under their experimental conditions.[31] Recently, Ding and co-workers have studied the catalytic performance of $[Ni(H_2O)_2(\gamma\text{-}SiW_{10}O_{35})_2]^{10-}$, and no catalytic activity was observed either in the similar $[Ru(bpy)_3]^{2+}$/visible-light illumination/$Na_2S_2O_8$ water oxidation system.[40]

In addition, we have performed the control experiments only in the absence of **1**−**3** under the same experimental conditions. A maximum value of 0.19 μmol O_2 was evolved after 60 min irradiation, suggesting that compounds **1**−**3** are catalytically active and can effectively promote the O_2 evolution in the water oxidation process. Furthermore, without photosensitizer $[Ru(bpy)_3]^{2+}$ or $Na_2S_2O_8$ sacrificial electron acceptor, there was no O_2 evolution even in the presence of **1**−**3**.

Table 1. Visible Light-Driven O_2 Evolution Catalyzed by Different Nickel Containing POM-Based WOCs

catalyst	TON[c]	TOF $[s^{-1}]^d$	ref
compound **1**[a]	85.6	0.13	this work
compound **2**[a]	94.1	0.15	this work
compound **3**[a]	124.4	0.21	this work
$[Ni_4(H_2O)_2(PW_9O_{34})_2]^{10-a}$	0	0	this work
$[Ni_4(H_2O)_2(SiW_9O_{34})_2]^{12-a}$	0	0	this work
$[Ni(H_2O)_2(\gamma\text{-}SiW_{10}O_{35})_2]^{10-}$	0	0	ref 40
$[Ni_5(OH)_6(OH_2)_3(Si_2W_{18}O_{66})]^{12-b}$	ca. 60	~0.18	ref 35

[a]Conditions: 300W Xe lamp equipped with a long-pass filter (420 nm cutoff); catalysts concentration (2 μM), $[Ru(bpy)_3]^{2+}$ (1.0 mM), $Na_2S_2O_8$ (5.0 mM), borate buffer (80 mM, pH 9.0), total reaction solution volume: 20 mL; vigorous stirring (1.5×10^3 rpm). [b]Conditions: catalyst concentration (2 μM), 455 nm LED light (17 mW, beam volume 2.0 mL). [c]TON = mol of O_2/mol of catalyst. [d]TOF = mol of O_2/(mol of catalyst × 300 s).

In order to understand the active photocatalytic property of compounds **1**−**3**, we attempt to look for answers from the band gap structures and crystal structural features of these Ni-containing POM compounds. First, the band gap structures of all three compounds were confirmed by the measurements of electrochemistry and the solid-state UV−vis spectra (Figure S12, S13 and Table S7 in SI). The HOMO of $[Ni_4(H_2O)_2(PW_9O_{34})_2]^{10-}$ and compounds **1**−**3** are +2.13, +1.85, +1.83 and +1.74 V, respectively. The potential difference (ΔE = HOMO $(Ru(bpy)_3)$ − HOMO (POMs)) between $Ru(bpy)_3$ and POMs increases with the order of ΔE ($[Ni_4(H_2O)_2(PW_9O_{34})_2]^{10-}$) < ΔE (compound **1**) < ΔE (compound **2**) < ΔE (compound **3**), indicating that the compounds from $[Ni_4(H_2O)_2(PW_9O_{34})_2]^{10-}$, **1**, **2** to **3** could be more and more easily oxidized by $Ru(bpy)_3$. As a result, the charge transfer efficiencies between $Ru(bpy)_3$ and POMs might increase in the order of $[Ni_4(H_2O)_2(PW_9O_{34})_2]^{10-}$ < compound **1** < compound **2** < compound **3**. Second, with the increase of Ni nuclearity, more catalytic active sites seem to be introduced into the POM-based molecular catalysts. At least in this case, the increase of nuclearity enhance the photocatalytic activities of compounds **1**−**3**. Moreover, in the structure point of view, when the plate-like $\{Ni_4\}$ moiety in $[Ni_4(H_2O)_2(PW_9O_{34})_2]^{10-}$ anion changed into quasi-cubane/cubane-like $\{Ni_3O_3\}/\{Ni_4O_4\}$ fragment in compounds **1**−**3**, more $\{Ni_xO_y\}$ fragments are exposed (see Figure S3, SI), which may not only easily contact with $\{Ru(bipy)_3\}$ and water molecules, but also tend to assemble into high nuclear Ni clusters, in favor of adjusting the band gap structures of POM compounds. Thus, the band gap structures, the number of catalytic active sites and the structural motif of POM compounds might be three key factors to influence the photocatalytic activity of POM-based WOCs.

Reuse of Catalysts 1−3. According to the recent publications, the reuse of catalysts **1**−**3** (5 μM) was carried out by addition of another 5 mM of $Na_2S_2O_8$ to the reaction solution after the first completion of catalytic experiment.[26,30,38−40] As shown in Figure S5 in SI, the evolved O_2 amount for the second run decreased to 4.2, 4.8 and 5.6 μmol for **1**−**3**, respectively. The pH values after the first run of photocatalytic experiments were 8.87 for **1**, 8.85 for **2**, and 8.82 for **3**. And the pH values after the second run changed into 8.48

DOI: 10.1021/jacs.5b01329
J. Am. Chem. Soc. 2015, 137, 5486−5493

for **1**, 8.45 for **2**, and 8.39 for **3**, respectively. The decline of the O_2 evolution activity after the first run suggests that such a photocatalytic reaction system is influenced by a combination of several factors (e.g., pH value changes and partial decomposition of the photosensitizer $[Ru(bpy)_3]^{2+}$) of the complicated solution environment.[33,40]

Catalysts Stability Tests. POMs, as one class of unique metal−oxo clusters, are composed of W, Mo, V, Nb, and Ta centers with their highest oxidation states. Thus, POMs can easily sustain the harsh oxidizing environment in the solar photoredox process. However, the hydrolytic stability of POMs may be influenced by a number of factors such as pH and buffer type and sometimes may decompose into catalytically active oxide nanoparticles.[61−65] In this work, we tested the stability of compounds **1**−**3** in aqueous solution by multiple experiments including DLS, UV−vis spectroscopy, catalysts aged experiments, tetra-*n*-heptylammonium nitrate ($THpANO_3$) toluene extraction, and the capillary electrophoretic method.

DLS measurements were performed in an 80 mM aqueous borate buffer solution (pH 9.0) containing 10 μM $Ni(NO_3)_2\cdot 6H_2O$, $[Ru(bpy)_3]^{2+}$ (1 mM), and $Na_2S_2O_8$ (5 mM) after 10 min irradiation. The DLS results showed nanoparticles with a diameter of 130.3 nm were readily detected (Figure S16, SI). The results confirmed that the formation of NiO_x nanoparticles from $Ni(NO_3)_2\cdot 6H_2O$ is effectively promoted upon the visible light irradiation. However, when the same experiments were conducted by using 5 μM **1**−**3**, no nanoparticles can be detected after 60 min of irradiation (Figure S14a, S14c and S14e in SI). These results indicate that compounds **1**−**3** did serve as molecular catalysts and did not decompose into NiO_x nanoparticles (especially nickel hydroxide/oxide nanoparticles) during the visible light-driven water oxidation.

UV−vis spectra of compounds **1**−**3** (1.0×10^{-4} M) were also performed in pH 9.0 sodium borate buffer solution (80 mM) with different aging time (0−90 min). As shown in Figure S17 in SI, the absorption peaks in these UV−vis spectra showed almost no change during a 90 min course of aging. The UV−vis spectra of compounds **1**−**3** (1.0×10^{-4} M) were also performed in pH 9.0 sodium borate buffer solution (80 mM) with $Na_2S_2O_8$ (5 mM) at different aging time (0−90 min). The UV−vis absorption spectra remained unchanged, suggesting that a strong oxidation environment has no impact on the stability of compounds **1**−**3** (see Figure S18 in SI). These results supported the stabilities of compounds **1**−**3** under the photocatalytic water oxidation process.

Moreover, $THpANO_3$ toluene extraction experiments were performed to quantitatively extract the compounds **1**−**3** from the aqueous solution. POM species with highly anionic nature can be well extracted by $THpA^+$ phase-transfer agent and the remaining soluble species in aqueous solution could be easily quantified by elemental analysis as reported by Hill and co-workers.[65] After extraction of compounds **1**−**3** from the aqueous solutions, inductively coupled plasma mass spectrometry (ICP-MS) was performed to quantify the amount of Ni-containing species remaining in solution. Aging 3 μM of compounds **1**−**3** in pH 9.0 sodium borate buffer (80 mM) for 12 h, followed by the extraction technique, 1.70, 1.35, and 2.73 μM of Ni concentrations were detected for compounds **1**−**3**, respectively (see Table S8, SI), while the corresponding W concentrations are 2.03, 0.66, and 1.74 μM for these solutions, respectively. The $THpANO_3$ toluene extraction experiments were also carried out after the photocatalytic water oxidation with 5 μM **1**−**3**. After 60 min of irradiation, the reaction solutions were aged for 10 h followed by the extraction technique. A concentration of nickel at 1.03, 1.15, and 2.36 μM remained in the reaction solution for compounds **1**, **2** and **3**, respectively. The corresponding W concentrations are 1.55, 1.12, and 1.4 μM for these solutions, respectively (see Table S9, SI). Further, aging 5 μM of compounds **1**−**3** in pH 9.0 sodium borate buffer (80 mM) for 8 h with $Na_2S_2O_8$ (5 mM) and then were taken for the photocatalytic water oxidation reaction. After 60 min of irradiation, the reaction solutions were extracted. The amount of nickel of 1.69, 1.51, and 2.65 μM remained in the reaction solution for compounds **1**, **2** and **3**, respectively. And, the corresponding W concentrations are 2.79, 2.04, and 3.21 μM for these solutions, respectively (Table S10, SI). These POM extraction and ICP-MS analysis results indicated that less than <4.7% of POMs could have decomposed to release Ni^{2+} ions in the borate buffer. To rule out that the contribution of dissociated Ni^{2+} ions to the observed photocatalytic water oxidation activities of compounds **1**−**3**, we further carried out the catalytic reaction with different concentrations of $Ni(NO_3)_2\cdot 6H_2O$ (1−10 μM) under the same catalytic conditions. As shown in Figure S6−S10 in SI, compounds **1**−**3** exhibited higher catalytic activity than the control Ni^{2+} ions. These control experiments demonstrated that minimum Ni^{2+} ions just produced a very small amount of O_2 and can not affect the photocatalytic activities of compounds **1**−**3**.

The capillary electrophoretic method has also been used to investigate the stability of compounds **1**−**3** in solution. This technique was designed to separate species based on their charge to size ratio in the interior of a small capillary filled with an electrolyte.[66,67] As shown in Figure S19, the peaks of compounds **1**−**3** have almost no changes before and after photocatalytic reactions except a light shift. This shift was caused by the change of electrolyte concentration before and after the visible light-driven water oxidation reactions. No additional new peaks were observed for compounds **1**−**3** before and after photocatalytic reactions. On the basis of all above experiments, we can envision that compounds **1**−**3** are structurally stable in solution during the water oxidation reactions.

We also conducted the photocatalytic water oxidation reactions after compounds **1**−**3** aged for 4, 8, and 12 h. The photocatalytic performances were almost the same as that of the fresh catalyst, respectively (see Figure S20 in SI). These experiments further proved that compounds **1**−**3** are stable under the visible light-driven water oxidation process.

■ CONCLUSIONS

Three new POM-based Ni clusters were synthesized, exhibiting the central $\{Ni_{12}\}$ (for **1**), $\{Ni_{13}\}$ (for **2**) and $\{Ni_{25}\}$ (for **3**) cores encapsulated by the lacunary $\{A\text{-}\alpha\text{-}SiW_9O_{34}\}$ POM units and the inorganic $\{PO_4\}$ and/or $\{CO_3\}$ ligands. Compound **3** represents the currently largest POM-based Ni cluster. All three compounds contain the $\{Ni_3O_3\}$ quasi-cubane or $\{Ni_4O_4\}$ cubane cores, which not only are structurally similar to the natural oxygen-evolving center $\{Mn_4O_5Ca\}$, but also show good catalytic activities in the visible light-driven water oxidation process. Compounds **1**−**3** as the homogeneous catalysts for visible light-driven water oxidation exhibit a high TON of 128.2 for **1**, 147.6 for **2**, and 204.5 for **3**, respectively. Furthermore, the photocatalytic efficiencies follow the order of **1** < **2** < **3**. The active photocatalytic property of compounds **1**−**3** was initially explained by virtue of the band gap structures, the number of catalytic active sites and the structural motif of

DOI: 10.1021/jacs.5b01329
J. Am. Chem. Soc. 2015, 137, 5486−5493

POM compounds, which might be three key factors to influence the photocatalytic activity of POM-based WOCs. Multiple experiments including DLS, UV−vis absorption, catalysts aged experiments, $THpANO_3$ toluene extraction, and capillary electrophoretic measurements confirmed that compounds **1**−**3** are structurally stable and the dominant active catalysts in the water oxidation system. This work shows the high feasibility of Ni-containing POMs as effective WOCs, which may pave new ways for further design and synthesis of more active POM-based WOCs in the near future. The relevant study is ongoing in our group.

■ ASSOCIATED CONTENT

Supporting Information

X-ray crystallography, additional structural figures, photocatalytic water oxidation experiments and EDX analysis, DLS, $THpANO_3$ toluene extraction experiments, UV−vis spectra, capillary electrophoretic measurements, IR spectra, TG curves and CIF files. This material is available free of charge via the Internet at http://pubs.acs.org.

■ AUTHOR INFORMATION

Corresponding Authors

*liyg658@nenu.edu.cn
*wangeb889@nenu.edu.cn

Notes

The authors declare no competing financial interest.

■ ACKNOWLEDGMENTS

This work was supported by the National Natural Science Foundation of China (21271039/21101022), Science and Technology Development Project Foundation of Jilin Province (20150520001JH), and Program for New Century Excellent Talents in University (Grant No. NCET120813).

■ REFERENCES

(1) Rüttinger, W.; Dismukes, G. C. *Chem. Rev.* **1997**, *97*, 1.
(2) Limburg, J.; Vrettos, J. S.; Liable-Sands, L. M.; Rheingold, A. L.; Crabtree, R. H.; Brudvig, G. W. *Science* **1999**, *283*, 1524.
(3) Youngblood, W. J.; Lee, S.-H. A.; Kobayashi, Y.; Hernandez-Pagan, E. A.; Hoertz, P. G.; Moore, T. A.; Moore, A. L.; Gust, D.; Mallouk, T. E. *J. Am. Chem. Soc.* **2009**, *131*, 926.
(4) Duan, L. L.; Bozoglian, F.; Mandal, S.; Stewart, B.; Privalov, T.; Llobet, A.; Sun, L. C. *Nat. Chem.* **2012**, *4*, 418.
(5) Young, K. J.; Martini, L. A.; Milot, R. L.; Snoeberger, R. C.; Batista, V. S.; Schmuttenmaer, C. A.; Crabtree, R. H.; Brudvig, G. W. *Coord. Chem. Rev.* **2012**, *256*, 2503.
(6) Kärkäs, M. D.; Verho, O.; Johnston, E. V.; Åkermark, B. *Chem. Rev.* **2014**, *114*, 11863.
(7) Kim, T. W.; Choi, K.-S. *Science* **2014**, *343*, 990.
(8) Parent, A. R.; Sakai, K. *ChemSusChem* **2014**, *7*, 2070.
(9) Dismukes, G. C.; Brimblecombe, R.; Felton, G. A. N.; Pryadun, R. S.; Sheats, J. E.; Spiccia, L.; Swiegers, G. F. *Acc. Chem. Res.* **2009**, *42*, 1935.
(10) Nocera, D. G. *Acc. Chem. Res.* **2012**, *45*, 767.
(11) McCool, N. S.; Robinson, D. M.; Sheats, J. E.; Dismukes, G. C. *J. Am. Chem. Soc.* **2011**, *133*, 11446.
(12) Hocking, R. K.; Brimblecombe, R.; Chang, L.-Y.; Singh, A.; Cheah, M. H.; Glover, C.; Casey, W. H.; Spiccia, L. *Nat. Chem.* **2011**, *3*, 461.
(13) Indra, A.; Menezes, P. W.; Zaharieva, I.; Baktash, E.; Pfrommer, J.; Schwarze, M.; Dau, H.; Driess, M. *Angew. Chem., Int. Ed.* **2013**, *52*, 13206.
(14) Fillol, J. L.; Codolà, Z.; Garcia-Bosch, I.; Gómez, L.; Pla, J. J.; Costas, M. *Nat. Chem.* **2011**, *3*, 807.
(15) Panda, C.; Debgupta, J.; Díaz, D. D.; Singh, K. K.; Gupta, S. S.; Dhar, B. B. *J. Am. Chem. Soc.* **2014**, *136*, 12273.
(16) Zhang, M.; Respinis, M.; Frei, H. *Nat. Chem.* **2014**, *6*, 362.
(17) Zhang, B. B.; Li, F.; Yu, F. S.; Wang, X. H.; Zhou, X.; Li, H.; Jiang, Y.; Sun, L. C. *ACS Catal.* **2014**, *4*, 804.
(18) Bediako, D. K.; Lassalle-Kaiser, B.; Surendranath, Y.; Yano, J.; Yachandra, V. K.; Nocera, D. G. *J. Am. Chem. Soc.* **2012**, *134*, 6801.
(19) Zhang, M.; Zhang, M.-T.; Hou, C.; Ke, Z.-F.; Lu, T.-B. *Angew. Chem., Int. Ed.* **2014**, *53*, 13042.
(20) Barnett, S. M.; Goldberg, K. I.; Mayer, J. M. *Nat. Chem.* **2012**, *4*, 498.
(21) Zhang, T.; Wang, C.; Liu, S. B.; Wang, J.-L.; Lin, W. B. *J. Am. Chem. Soc.* **2014**, *136*, 273.
(22) Gao, M. R.; Sheng, W. C.; Zhuang, Z. B.; Fang, Q. R.; Gu, S.; Jiang, J.; Yan, Y. S. *J. Am. Chem. Soc.* **2014**, *136*, 7077.
(23) Kinoshita, K. *Electrochemical Oxygen Technology*; Wiley-Interscience: New York, 1992.
(24) Geletii, Y. V.; Botar, B.; Kögerler, P.; Hillesheim, D. A.; Musaev, D. G.; Hill, C. L. *Angew. Chem., Int. Ed.* **2008**, *47*, 3896.
(25) Sartorel, A.; Carraro, M.; Scorrano, G.; Zorzi, R. D.; Geremia, S.; McDaniel, N. D.; Bernhard, S.; Bonchio, M. *J. Am. Chem. Soc.* **2008**, *130*, 5006.
(26) Geletii, Y. V.; Huang, Z.; Hou, Y.; Musaev, D. G.; Lian, T.; Hill, C. L. *J. Am. Chem. Soc.* **2009**, *131*, 7522.
(27) Toma, F. M.; Sartorel, A.; Iurlo, M.; Carraro, M.; Parisse, P.; Maccato, C.; Rapino, S.; Gonzalez, B. R.; Amenitsch, H.; Ros, T. D.; Casalis, L.; Goldoni, A.; Marcaccio, M.; Scorrano, G.; Scoles, G.; Paolucci, F.; Prato, M.; Bonchio, M. *Nat. Chem.* **2010**, *2*, 826.
(28) Yin, Q. S.; Tan, J. M.; Besson, C.; Geletii, Y. V.; Musaev, D. G.; Kuznetsov, A. E.; Luo, Z.; Hardcastle, K. I.; Hill, C. L. *Science* **2010**, *328*, 342.
(29) Murakami, M.; Hong, D.; Suenobu, T.; Yamaguchi, S.; Ogura, T.; Fukuzumi, S. *J. Am. Chem. Soc.* **2011**, *133*, 11605.
(30) Huang, Z. Q.; Luo, Z.; Geletii, Y. V.; Vickers, J. W.; Yin, Q. S.; Wu, D.; Hou, Y.; Ding, Y.; Song, J.; Musaev, D. G.; Hill, C. L.; Lian, T. Q. *J. Am. Chem. Soc.* **2011**, *133*, 2068.
(31) Car, P.-E.; Guttentag, M.; Baldridge, K. K.; Albertoa, R.; Patzke, G. R. *Green Chem.* **2012**, *14*, 1680.
(32) Lv, H.; Geletii, Y. V.; Zhao, C.; Vickers, J. W.; Zhu, G.; Luo, Z.; Song, J.; Lian, T.; Musaev, D. G.; Hill, C. L. *Chem. Soc. Rev.* **2012**, *41*, 7572.
(33) Tanaka, S.; Annaka, M.; Sakai, K. *Chem. Commun.* **2012**, *48*, 1653.
(34) Goberna-Ferrón, S.; Vigara, L.; Soriano-López, J.; Galán-Mascarós, J. R. *Inorg. Chem.* **2012**, *51*, 11707.
(35) Zhu, G. B.; Glass, E. N.; Zhao, C. C.; Lv, H. J.; Vickers, J. W.; Geletii, Y. V.; Musaev, D. G.; Song, J.; Hill, C. L. *Dalton Trans.* **2012**, *41*, 13043.
(36) Bernardini, G.; Wedd, A. G.; Zhao, C.; Bond, A. M. *Proc. Natl. Acad. Sci. U. S. A.* **2012**, *109*, 11552.
(37) Symes, M. D.; Cronin, L. *Nat. Chem.* **2013**, *5*, 403.
(38) Song, F. Y.; Ding, Y.; Ma, B. C.; Wang, C. M.; Wang, Q.; Du, X. Q.; Fu, S.; Song, J. *Energy Environ. Sci.* **2013**, *6*, 1170.
(39) Han, X.-B.; Zhang, Z.-M.; Zhang, T.; Li, Y.-G.; Lin, W.; You, W.; Su, Z.-M.; Wang, E.-B. *J. Am. Chem. Soc.* **2014**, *136*, 5359.
(40) Xiang, R.; Ding, Y.; Zhao, J. W. *Chem.—Asian J.* **2014**, *9*, 3228.
(41) Lv, H.; Song, J.; Geletii, Y. V.; Vickers, J. W.; Sumliner, J. M.; Musaev, D. G.; Kögerler, P.; Zhuk, P. F.; Bacsa, J.; Zhu, G.; Hill, C. L. *J. Am. Chem. Soc.* **2014**, *136*, 9268.
(42) Santoni, M.-P; La Ganga, G.; Nardo, V. M.; Natali, M.; Puntoriero, F.; Scandola, F.; Campagna, S. *J. Am. Chem. Soc.* **2014**, *136*, 8189.
(43) Al-Oweini, R.; Sartorel, A.; Bassil, B. S.; Natali, M.; Berardi, S.; Scandola, F.; Kortz, U.; Bonchio, M. *Angew. Chem., Int. Ed.* **2014**, *53*, 11182.
(44) Xiao, F. P.; Hao, J.; Zhang, J.; Lv, C. L.; Yin, P. C.; Wang, L. S.; Wei, Y. G. *J. Am. Chem. Soc.* **2010**, *132*, 5956.
(45) Lydon, C.; Sabi, M. M.; Symes, M. D.; Long, D.-L.; Murrie, M.; Yoshii, S.; Nojiri, H.; Cronin, L. *Chem. Commun.* **2012**, *48*, 9819.

DOI: 10.1021/jacs.5b01329
J. Am. Chem. Soc. 2015, 137, 5486−5493

(46) Niu, J.; Li, F.; Zhao, J.; Ma, P.; Zhang, D.; Bassil, B. S.; Kortz, U.; Wang, J. *Chem.—Eur. J.* **2014**, *20*, 9852.
(47) Anderson, T. M.; Rodriguez, M. A.; Bonhomme, F.; Bixler, J. N.; Alam, T. M.; Nyman, M. *Dalton Trans.* **2007**, *40*, 4517.
(48) Huang, P.; Qin, C.; Su, Z. M.; Xing, Y.; Wang, X. L.; Shao, K. Z.; Lan, Y. Q.; Wang, E. B. *J. Am. Chem. Soc.* **2012**, *134*, 14004.
(49) Zheng, S.-T.; Yang, G.-Y. *Chem. Soc. Rev.* **2012**, *41*, 7623.
(50) Oms, O.; Dolbecq, A.; Mialane, P. *Chem. Soc. Rev.* **2012**, *41*, 7497.
(51) Ibrahim, M.; Haider, A.; Lan, Y.; Bassil, B. S.; Carey, A. M.; Liu, R.; Zhang, G.; Keita, B.; Li, W.; Kostakis, G. E.; Powell, A. K.; Kortz, U. *Inorg. Chem.* **2014**, *53*, 5179.
(52) Besson, C.; Huang, Z.; Geletii, Y. V.; Lense, S.; Hardcastle, K. I.; Musaev, D. G.; Lian, T.; Proust, A.; Hill, C. L. *Chem. Commun.* **2010**, *46*, 2784.
(53) Gao, J. K.; Cao, S. W.; Tay, Q. L.; Liu, Y.; Yu, L. M.; Ye, K. Q.; Mun, P. C. S.; Li, Y. X.; Rakesh, G.; Loo, S. C. J.; Chen, Z.; Zhao, Y.; Xue, C.; Zhang, Q. C. *Sci. Rep.* **2013**, *3*, 1853.
(54) Kupitz, C.; Basu, S.; Grotjohann, I.; Fromme, R.; Zatsepin, N. A.; Rendek, K. N.; Hunter, M. S.; Shoeman, R. L.; White, T. A.; Wang, D.; James, D.; Yang, J.-H.; Cobb, D. E.; Reeder, B.; Sierra, R. G.; Liu, H.; Barty, A.; Aquila, A. L.; Deponte, D.; Kirian, R. A.; Bari, S.; Bergkamp, J. J.; Beyerlein, K. R.; Bogan, M. J.; Caleman, C.; Chao, T.-C.; Conrad, C. E.; Davis, K. M.; Fleckenstein, H.; Galli, L.; Hau-Riege, S. P.; Kassemeyer, S.; Laksmono, H.; Liang, M.; Lomb, L.; Marchesini, S.; Martin, A. V.; Messerschmidt, M.; Milathianaki, D.; Nass, K.; Ros, A.; Roy-Chowdhury, S.; Schmidt, K.; Seibert, M.; Steinbrener, J.; Stellato, F.; Yan, L.; Yoon, C.; Moore, T. A.; Moore, A. L.; Pushkar, Y.; Williams, G. J.; Boutet, S.; Doak, R. B.; Weierstall, U.; Frank, M.; Chapman, H. N.; Spence, J. C. H.; Fromme, P. *Nature* **2014**, *513*, 261.
(55) Hervé, G.; Tézé, A. *Inorg. Chem.* **1977**, *16*, 2115.
(56) Sheldrick, G. M. *SHELXL97, Program for Crystal Structure Refinement*; University of Göttingen: Göttingen, Germany, 1997. Sheldrick, G. M. *SHELXS97, Program for Crystal Structure Solution*; University of Göttingen: Göttingen, Germany, 1997.
(57) Zhang, H.-M.; Li, Y.-G.; Lu, Y.; Clérac, R.; Zhang, Z.-M.; Wu, Q.; Feng, X.-J.; Wang, E.-B. *Inorg. Chem.* **2009**, *48*, 10889.
(58) Ibrahim, M.; Xiang, Y. X.; Bassil, B. S.; Lan, Y. H.; Powell, A. K.; Oliveira, P.; Keita, B.; Kortz, U. *Inorg. Chem.* **2013**, *52*, 8399.
(59) Hara, M.; Waraksa, C. C.; Lean, J. T.; Lewis, B. A.; Mallouk, T. E. *J. Phys. Chem. A* **2000**, *104*, 5275.
(60) Morris, N. D.; Mallouk, T. E. *J. Am. Chem. Soc.* **2002**, *124*, 11114.
(61) Stracke, J. J.; Finke, R. G. *J. Am. Chem. Soc.* **2011**, *133*, 14872.
(62) Natali, M.; Berardi, S.; Sartorel, A.; Bonchio, M.; Campagna, S.; Scandola, F. *Chem. Commun.* **2012**, *48*, 8808.
(63) Stracke, J. J.; Finke, R. G. *ACS Catal.* **2013**, *3*, 1209.
(64) Stracke, J. J.; Finke, R. G. *ACS Catal.* **2014**, *4*, 79.
(65) Vickers, J. W.; Lv, H. J.; Sumliner, J. M.; Zhu, G. B.; Luo, Z.; Musaev, D. G.; Geletii, Y. V.; Hill, C. L. *J. Am. Chem. Soc.* **2013**, *135*, 14110.
(66) Himeno, S.; Kitazumi, I.; Takamoto, M.; Nakashima, Y. *Talanta* **2003**, *61*, 591.
(67) Himeno, S.; Kitano, E.; Kanaya, M.; Takamoto, M. *Talanta* **2007**, *71*, 822.

DOI: 10.1021/jacs.5b01329
J. Am. Chem. Soc. 2015, 137, 5486−5493